2023

Analytical chemical methods for advanced and environmental materials. — High-resolution continuum source atomic absorption spectrometry (HR-CS-AAS) using graphite furnace atomization with solid (powder) and solution sampling were developed and applied to quantitate various dopant elements (Bi, Mg) and impurities (Fe) from microsamples of optical crystals of lithium niobate and raw growth materials. Flame HR-CS-AAS methods were developed with matrix-matching to check the accuracy of the methodology.
Some low-cost sensors (LCSs) were compared for different aerosol size ranges with a research-grade instrument under controlled laboratory conditions. An aerosol generator was utilized to produce various sizes of monodispersed particulate matter (PM), which was introduced into a laboratory smoke chamber under resistance heating/cooling and/or varying RH conditions. Besides, the accuracy of the air temperature (T) and relative humidity (RH) sensors of the LCSs were assessed against calibrated laboratory-grade instruments. The study LCSs showed generally accurate readings for $PM_{2.5}$, irrespectively of the slow T and/or RH changes, which provided apt conditions for calibration. On the other hand, PM_1 and PM_{10} readings slightly deviated from those observed with the reference monitor, likely due to the lower detection efficacy of the formers towards fine and coarse PM. For T calibration, low RH in the smoke chamber provided more reproducible conditions in terms of the lower measurement bias for LCSs as recorded against a calibrated, reference-grade thermometer.

Bi-doped stoichiometric $LiNbO_3$ (SLN) crystals. – A temperature-controlled two-wave mixing setup was built up to investigate photorefractive and photochromic effects in Bi doped, and Bi-Mg co-doped stoichiometric lithium niobate single crystals at 405 nm. Since the second one has been recently shown to be a good candidate for 3D holographic displays, its practical application requires deep study of its photochromic properties besides the photorefractive ones. Beyond long-term photochromic effect we also found a wide time scale of decay components, down to the order of seconds. For this reason, only stretched exponential function can be fitted well to the time evolution of the absorption coefficients. A strong temperature dependence of the nominal time constants was also found with activation energies between 0.3 and 0.7 eV in both $LiNbO_3$:Bi and $LiNbO_3$:Bi,Mg samples. Lower activation energies were found in case of Mg co-doped crystals. Two-wave mixing experiments gave recording time of 25 ms for $LiNbO_3$:Bi,Mg, which is near to the same found in the literature for congruent crystals measured at 442 nm.
Formation of $LiNbO_3$ nanocrystals by solvothermal method – An easy and relatively low temperature solvothermal (bottom-up) method was optimized for preparing $LiNbO_3$ nanocrystals with homogenous particle size distribution 60-100 nm with a yield of 90 %. The effects of polyol media, reaction time and Li excess of the starting reagents were investigated. According to the X-ray diffraction phase analysis, Li_3NbO_4 and Nb_2O_5 have also been detected beside the LN phase in many samples depending on the ratio of the starting components and the reaction time. At 220 °C, the optimal synthesis parameters for the reaction of Nb_2O_5 with LiOH to form $LiNbO_3$ were found to be diethylene glycol as polyol medium and 72-hour reaction time. Independently of the polyol medium used, the lithium oxide up-take of the niobium(V) oxide grains started with the formation of a lithium-rich phase, Li_3NbO_4, very likely at the Nb_2O_5/solvent boundary, which was followed by the equilibration of the concentrations within the grains. For the accomplishment of the $LiNbO_3$ formation, a lithium oxide excess was necessary [1].

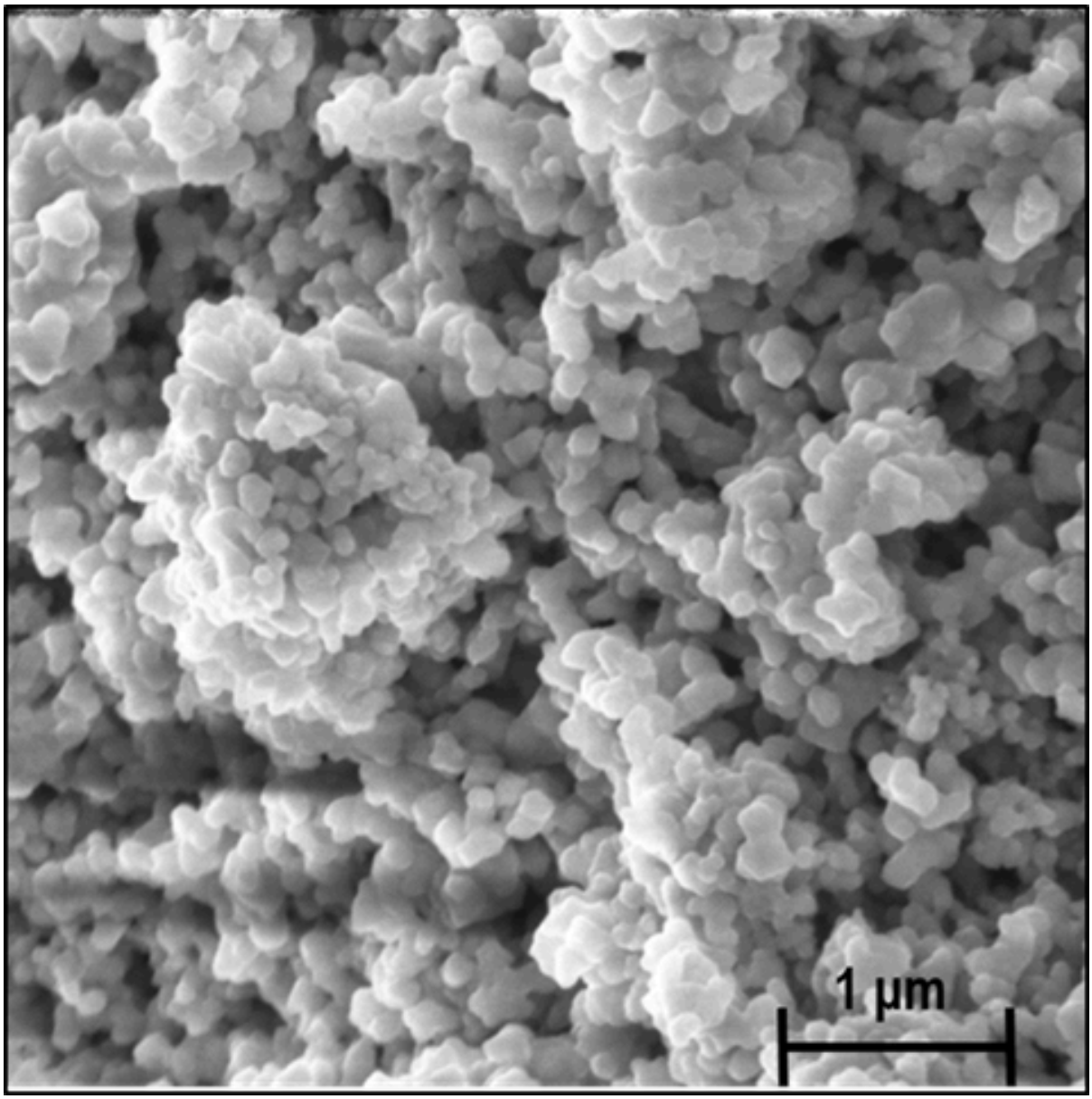

Figure 1. Typical SEM image of the LiNbO3 samples prepared by the solvothermal synthesis.

Preparation and investigation of $LiNb_{1-x}Ta_xO_3$ mixed crystals – Lithium niobate ($LiNbO_3$, LN) and lithium tantalate ($LiTaO_3$, LT) are uniaxial ferroelectric materials with high Curie temperatures and are characterized by a large spontaneous polarization. Due to their unusual large piezoelectric, electro-optic, and nonlinear coefficients they are employed for applications in linear and nonlinear integrated optics as well as surface acoustic wave generation. Because of the to the small ionic radius difference, Nb is easily substituted by the isoelectronic Ta, which allows for the fabrication of $LiNb_{1-x}Ta_xO_3$ mixed crystals over the complete compositional range creating the basis of the tunability of several physical composition dependent properties. Our goal was to produce homogeneous, crack- and inclusion-free monodomain crystals, to determine Ta/Nb in the axial and radial direction of the crystal and to investigate the composition-dependent spectroscopic properties. Mixed crystals were grown from the melt containing 5 mol% Ta. Due to the large difference in the melting points, between the LN seed and the melt containing 5 mol% Ta, cracks were visible at the beginning of the crystal. To prevent cracking, the seed of suitable composition was cut from the mixed crystal. After the next growth the crystal was successfully poled and turned to be monodomain. The Ta content was determined along with the growth (Y-cut) and the radial (Z-cut) axis with energy-dispersive X-ray spectrometry (EDS) in scanning electron microscope. The Ta content of the crystal decreases monotonically from top to bottom in the range of 15-10 mol%. The strongly differing optical absorption edge of congruent LN (320 nm) and LT (278 nm) may allow us also to follow the change of the [Ta]/[Nb] ratio in $LiNb_{1-x}Ta_xO_3$ mixed crystals. The absorption edge (wavelength at $\alpha = 20\ cm^{-1}$) has shifted to longer wavelength along the growing axis from the top to the bottom part of the crystal indicating a slightly decreasing Ta content similarly to the results of EDS.

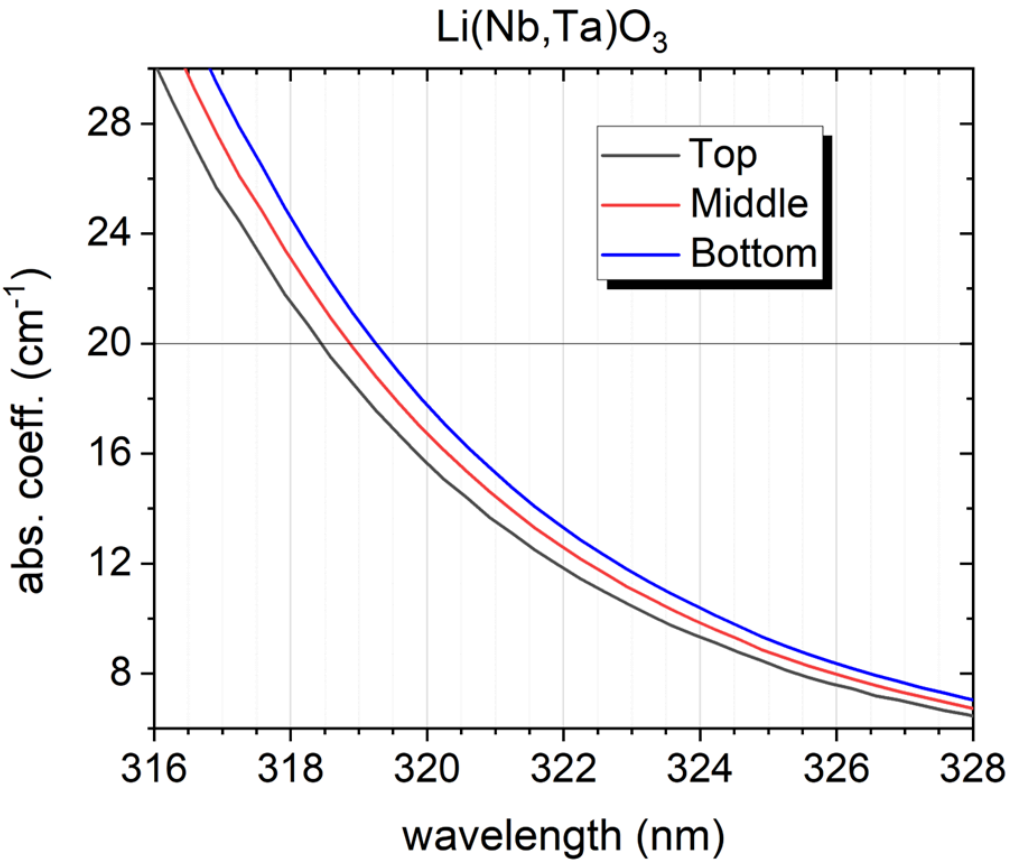

Figure 2. The absorption spectra of $LiNb_{1-x}Ta_xO_3$ sample plotted around the absorption edge to show the compositional change in the growing direction.

.

References

[1] G. Dravecz, T. Kolonits, L. Péter, Formation of $LiNbO_3$ Nanocrystals Using the Solvothermal Method, Crystals 13:1, 77, 10 p. (2023)

2022

Lithium niobate nanocrystals. – Congruent lithium niobate ($LiNbO_3$) prepared by sintering was ground under wet conditions in a planetary mill in order to produce nanocrystals. By using gradually smaller sizes of the balls in the mill, the final particle size of the crystals could be reduced to about 12–15 nm. The particle size achieved as well as the lithium oxide (Li_2O) loss of the lithium niobate particles were followed as a function of the grinding time. Lithium oxide was found to be released throughout the entire milling procedure, even during stages when the particle size changed no longer for a given ball size. About 12% and 20% Li_2O loss was detected upon grinding with 3 mm and 0.5 mm balls, respectively. X-ray diffractometry revealed the formation of a lithium-deficient phase, $LiNb_3O_8$; its presence was also confirmed by means of Raman spectroscopy. As derived from the diffractograms and from the lithium oxide loss determined by coulometric titration for a particle size of 70 nm, a $LiNb_3O_8$:$LiNbO_3$ volume ratio of 0.39 (± 0.03) was achieved. The composition change was found to be correlated with the total surface area of the particle assembly calculated from dynamic light scattering measurements. [1]

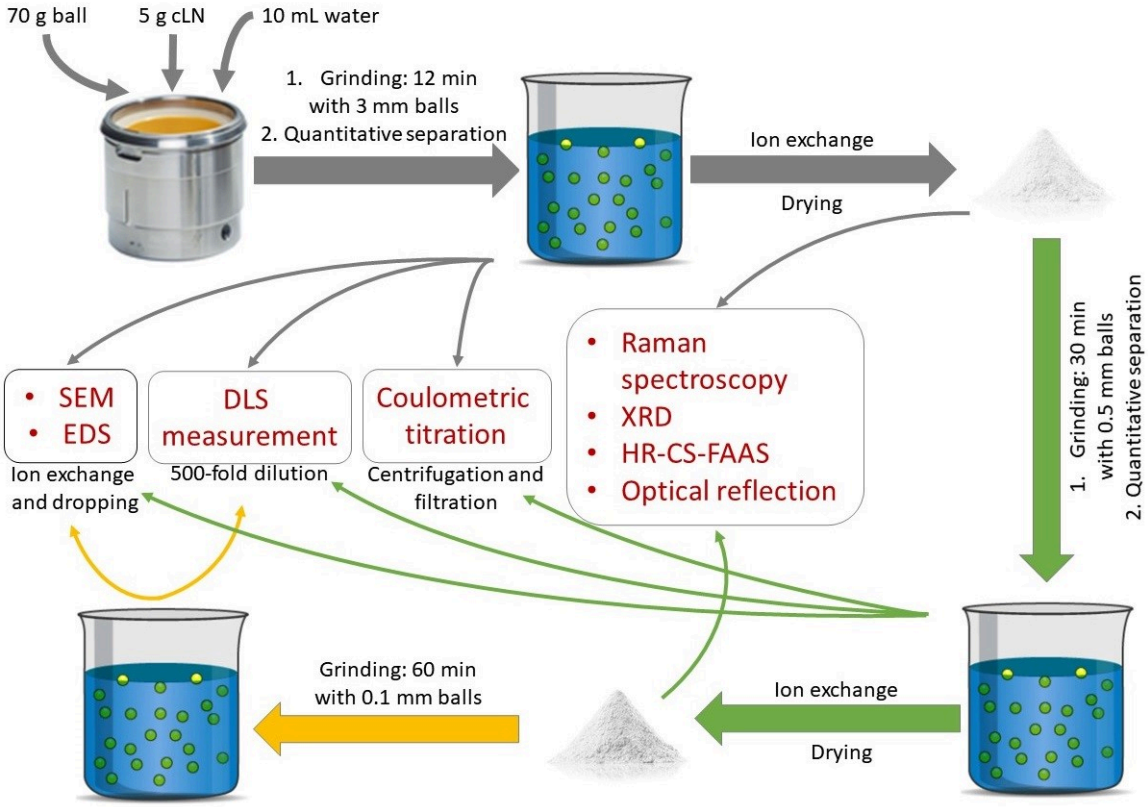

Organization chart of the sample preparation and characterization methods applied.

Single rare-earth ion quantum emitter in $LiNbO_3$ thin film. – Electro-optical control of on-chip photonic devices is an essential tool for efficient integrated photonics. Lithium niobate on insulator (LNOI) is an emerging platform for on-chip photonics due to its large electro-optic coefficient and high nonlinearity. The integration of quantum emitters into LNOI would extend their versatile use from classical photonics to quantum computing and communication. Single rare-earth ion (REI) quantum emitters have been incorporated into electro-optically tunable lithium niobate (LN) thin films; it has been demonstrated that the REI was able to control the coupled LN microcavities over a frequency range of up to 160 GHz with a switching time of 5 μs. The dynamical control of the cavities enabled the modulation of the Purcell enhancement of the REIs with short time constants. Using the Purcell enhancement evidence for the detection of single Yb^{3+} ions in the LN cavities has been obtained. The coupling of quantum emitters into fast tunable photonic devices is an efficient method to shape the waveform of the emitter. It also offers a platform to encode quantum information into an integrated spectral-temporal-spatial domain to achieve high levels of channel multiplexing as well as an approach to generate deterministic single-photon sources. [2]

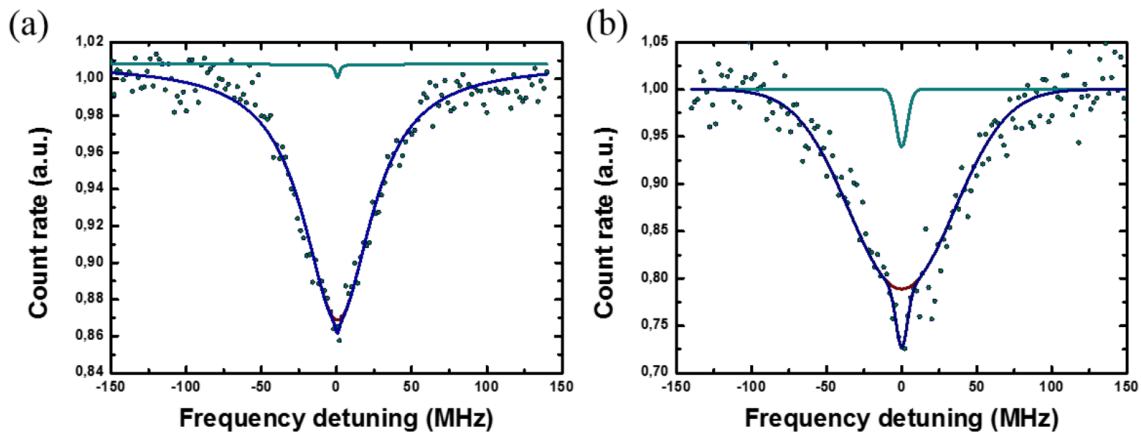

Spectral hole burning at 3.5 K and zero magnetic field of bulk Yb:LN (a) and implanted Yb in LN long waveguide (b).

Bi-doped stoichiometric $LiNbO_3$ (SLN) crystals. - Bismuth-doped lithium niobate (LN) is an excellent candidate for 3D holographic displays; congruent LN:Bi+Mg crystals in particular provide an essentially decreased reaction

time. Recently stoichiometric Bi and Bi+Mg doped crystals have been grown by the Czochralski and the high-temperature top-seeded solution growth methods. The defect structure induced by the dopants has been studied by UV-VIS and IR absorption spectroscopies. Although only a fraction of several thousandths of the amount of Bi added to the melt or solution was incorporated into the crystals, significant absorption has been observed in the UV range close to the absorption edge of the crystal. Additional absorption between 300-600 nm could also be induced by UV illumination but could be eliminated by a short anneal at ≥200-250 °C. The time constant of this photochromic effect was found to be an order of magnitude shorter for the Bi+Mg co-doped crystal as compared to SLN single-doped with Bi. As concluded from hydroxyl-ion spectra in the IR range bismuth ions occupy Li sites in single-Bi-doped crystals, while in double-doped SLN at least part of them may occupy Nb sites. The formation of excitons pinned at Bi complexes may be responsible for the new bands close to the UV edge, while further illumination may lead to further excitations of these pinned excitons. Detailed knowledge about these Bi-related defects may help to understand the photorefractive behaviour of Bi or Bi+Mg doped SLN crystals.

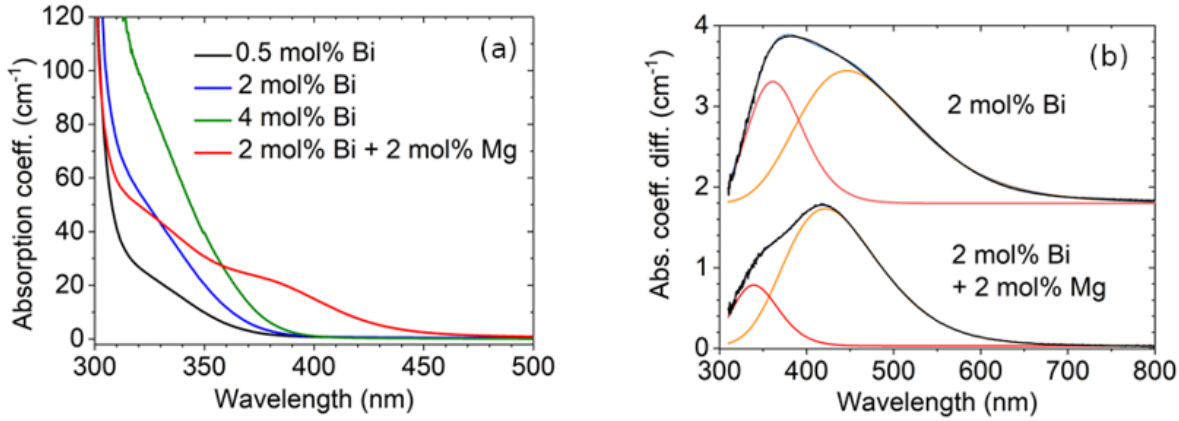

UV absorption bands in Bi and Bi+Mg doped SLN crystals grown by the Czochralski method (a). Additional photochromic absorption induced by UV light in Bi and Bi+Mg doped SLN crystals (b).

Yb and Er-doped Lithium Yttrium Ortoborate [Li6Y(BO3)3] single crystals. - A pump–probe type saturation spectroscopic experiment has been successfully employed to measure the relaxation parameters of the Yb^{3+}: $^2F_{7/2}$—$^2F_{5/2}$ and Er^{3+}: $^4I_{15/2}$—$^4I_{11/2}$ transitions in LYB single crystals in the temperature range of 2–14 and 9–28 K, respectively. The dipole and population relaxation times were found to be at about twice longer than those measured in stoichiometric or congruent lithium niobate single crystals, except for the dipole relaxation time of the narrow component in Yb^{3+} spectra where the increase was much larger. The nearly negligible perturbation caused by the neutral- charge substitution of the rare earth ions for Y in LYB crystals explains the longer population relaxation time as compared to lithium niobate. The difference in the dipole relaxation times can be understood by the fluctuating magnetic field, which seems to be stronger in $LiNbO_3$ due to the high nuclear magnetic moment of the Nb^{5+} ion. Although LYB as a host material seems to be better suited than $LiNbO_3$, the coherence time of excitation of the Yb^{3+} dopant is still much shorter than in Y_2SiO_5, and most likely there is a similar situation for the $^4I_{15/2}$—$^4I_{11/2}$ transition of the Er^{3+} dopant as well. [3]

Analytical chemical methods for advanced and environmental materials. — Solid sampling and solution introduction based microanalytical methods were developed and applied by means of high-resolution continuum source atomic absorption spectrometry to quantitate various metals from nanomaterials, bulk samples of optical crystals of lithium niobate, and plasma treated aqueous solutions. For instance, the dissolved content of Ca, Fe, Mg and Zn metals (applied as powders) formed during low-temperature surface microwave plasma treatment in aqueous solutions were determined, aiming at the study of formation and stabilization of reactive oxygen and nitrogen species (RONS) [4]. RONS have relevance for instance in cereal handling/storage in agriculture, due to their antimicrobial and antibacterial effects.

Low-cost air quality sensors (LCSs) were studied at urban, suburban and background sites in Budapest, to monitor PM1, PM2.5, PM10, and microclimatic parameters at high resolution (1 s to 5 min). These devices utilize the method of laser irradiation and multi-angle light scattering on air-suspended particulates. The LCSs showed acceptable accuracy for PM species in indoor/outdoor air even without use of external calibration. Low PM readings (<10 μg/m^3) were generally handicapped by higher bias, even between sensors of the same type. High relative humidity (>85%) slightly affected the PM readings of LCSs, necessitating field calibration. The LCSs were useful for detecting pollution stemming from emissions of motor vehicular traffic and residential cooking/heating activities [5].

Characteristic defects of stoichiometric $LiNbO_3$ grown by high-temperature top-seeded solution growth technique. — {01.8} faces have been identified in the bottom part of a stoichiometric $LiNbO_3$ crystal grown from

K_2O flux by the high-temperature top-seeded solution growth method. The faces were found to be related to the appearance of oppositely oriented domains. A SEM investigation of the domain areas after selective etching of the polished z-cut sample revealed a dislocation-related crystal defect beneath the surface.

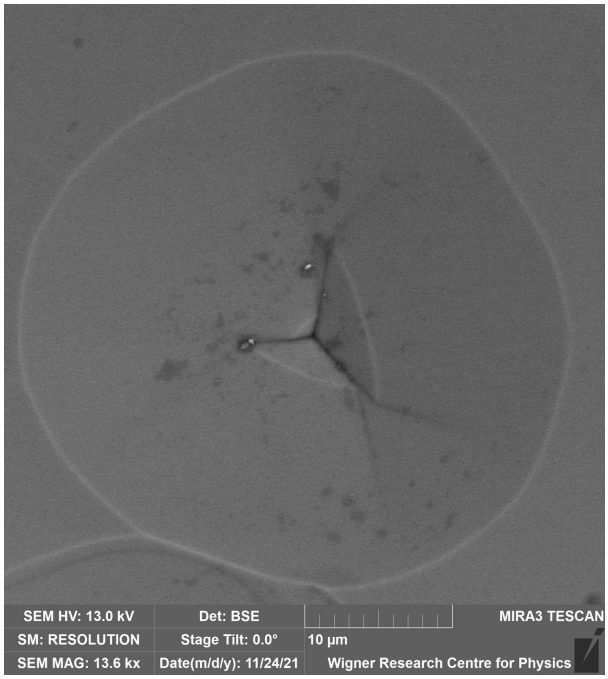

2021

$Li_6Y(BO_3)_3$ single crystals doped by Yb ions. – Cooperative luminescence (CL) of Yb^{3+} pairs was investigated in Yb-doped $Li_6Y(BO_3)_3$ crystals [1]. It was reliably distinguished from other types of up-conversion luminescence related to the energy transfer from Yb^{3+} ions to other rare-earth ions unintentionally introduced into the crystal. The CL was observed in the region of 19000–21000 cm^{-1} (526-476 nm) under excitation at about 10285 cm^{-1} (972.3 nm) by continuous wave or pulsed lasers. The emission band is nearly featureless at room temperature but develops a pronounced line spectrum at low temperatures. The width of the absorption line corresponding to the $^2F_{7/2} \rightarrow {}^2F_{5/2}$ transition of the Yb^{3+} ions at 10285 cm^{-1} demonstrates an extreme dependence on temperature, increasing by a factor of 250 from 6 to 300 K. The dependence of the CL intensity on laser irradiation power in the continuous wave mode is interpreted by an analytical model based on the intensity saturation effect strongly related to the peak amplitude of the absorption line. The model updates earlier descriptions of this dependence given in terms of power functions with “anomalous” exponents differing from the value of 2 expected for the luminescence of pair centres and accounts for the observed sharp temperature dependence of the saturation intensity. The decay kinetics of CL was shown to be approximately twice as fast as that of a single-ion luminescence, as expected. However, the decay times were found to be decreasing with increasing Yb concentration, which is explained by excitation escape from Yb^{3+} pairs due to energy transfer along Yb chains.

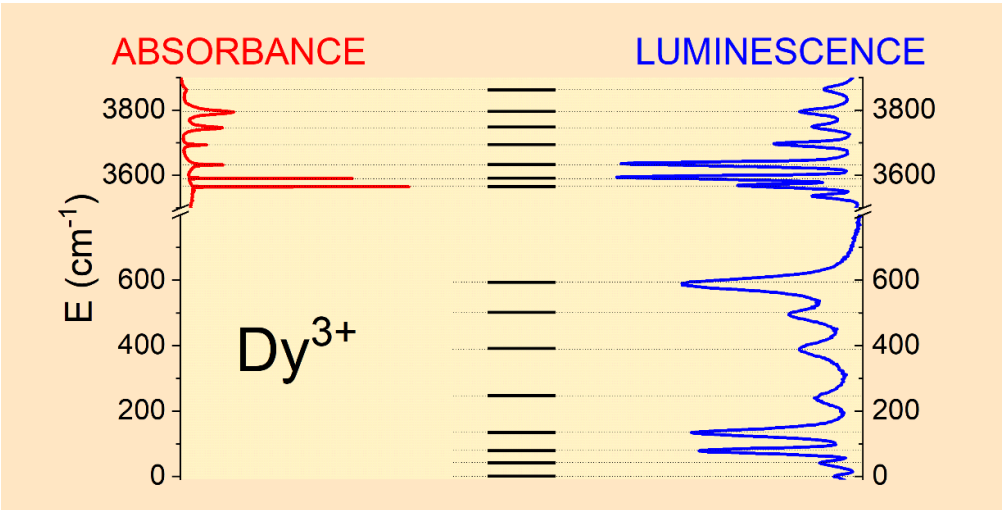

Figure 1. Crystal field splittings of the $^6H_{15/2}$ ground state and $^6H_{13/2}$ first excited state multiplets of Dy^{3+} ions in LYB crystals determined from the absorption and luminescence spectra.

$Li_6Y(BO_3)_3$ single crystals doped by Dy ions. – The energy levels of Dy^{3+} ions have been determined in lithium yttrium borate (Li6Y(BO3)3) single crystals (partly shown in Fig. 1) in a wide spectral range between 3000 and 40000 cm-1 using optical absorption and luminescence spectroscopy, which also allow for an analysis of the ground state [2]. The crystal field splittings of the $^6H_{15/2}$ ground state and all excited states up to the $^4F_{7/2}$ manifold were obtained at low temperature, based on luminescence (T = 4.2–78 K) and absorption (T = 8–100 K) measurements, respectively. The numbers of experimentally observed Stark sublevels are in agreement with those expected theoretically for Dy^{3+} ions occupying a single low symmetry (C1) site.

Polarons versus oxygen vacancies in LiNbO3. – We reviewed the resolution of the several decades-long controversy on the possible role of oxygen-vacancy defects in $LiNbO_3$ [3]. Confronting ideas of a selected series of papers from classical experiments to brand new large-scale calculations, a unified interpretation of the defect generation and annealing mechanisms governing processes during thermo- and mechanochemical treatments and irradiations of various types was presented. The dominant role of as-grown and freshly generated Nb antisite defects as traps for small polarons and bipolarons was demonstrated, while mobile lithium vacancies, also acting as hole traps, were shown to provide flexible charge compensation needed for stability. The close relationship between $LiNbO_3$ and the Li battery materials $LiNb_3O_8$ and Li_3NbO_4 was pointed out. The oxygen sublattice of the bulk plays a much more passive role, whereas oxygen loss and Li_2O segregation only take place in external or internal surface layers of a few nanometers.

Magnesium doped $LiNbO_3$ nanopowders. – Near-infrared (NIR) marker-based imaging is of growing importance for deep tissue imaging and is based on a considerable reduction of optical losses at large wavelengths. We aimed to extend the range of NIR excitation wavelengths particularly to values beyond 1.6 μm in order to profit from the low loss biological windows NIR-III and NIR-IV [4]. We addressed this task by studying NIR-excitation to NIR-emission conversion and imaging in the range of 1200 up to 2400 nm at the example of harmonic Mg-doped lithium niobate nanoparticles using (i) a nonlinear diffuse femtosecond-pulse reflectometer and (ii) a Tunable hIGh EneRgy (TIGER) widefield microscope. We successfully demonstrated the existence of appropriate excitation/emission configurations in this spectral region taking harmonic generation into account. Moreover, NIR-imaging using the most striking configurations, based on second harmonic generation (SHG) from NIR-III to NIR-I, or on third harmonic generation (THG) from NIR-IV to NIR-I, was demonstrated with excitation wavelengths 1.6–1.8 μm and 2.1–2.2 μm, respectively.

Cerium doped YSO and LYSO nanopowders. – Polycrystalline, cerium-doped yttrium oxyorthosilicate (Y_2SiO_5:Ce, YSO:Ce) and lutetium yttrium oxyorthosilicate ($Lu_{2-x}Y_xSiO_5$:Ce, LYSO:Ce) scintillator materials have been synthesized and characterized [5]. Samples have been prepared at 1400 °C with the aid of LiF flux. The initial concentration of the flux and the cerium content has strongly affected the particle size and photoluminescence (PL) intensity of the host crystal. Scanning electron microscopy (SEM) and dynamic light scattering (DLS) measurements have proven that the sizes of particles are in the range of 200–500 nm for powdered samples prepared with ≈18 mol% LiF concentration (Fig. 2). The highest PL yield for the X2-YSO phase has been observed for host crystals with 1 mol% Ce^{3+}. Increasing the Ce content in YSO and LYSO, as well as the Y content in LYSO samples resulted in a redshift in their PL emission spectra.

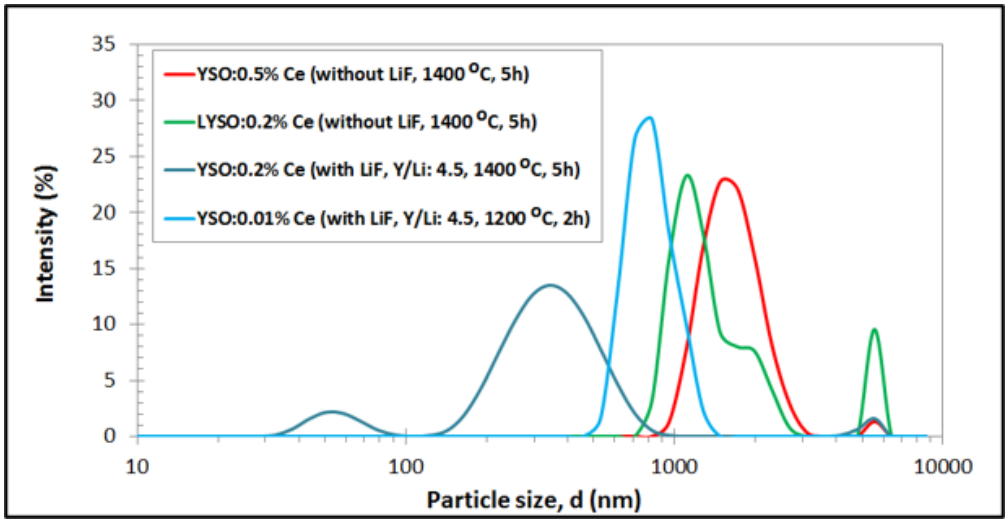

Figure 2. Average intensity versus particle size functions, determined with DLS for YSO and LYSO polycrystalline samples obtained under different synthesis conditions (varied pyrolysis temperature, Ce dopant and LiF additive content).

Chromium doped zinc gallate nanopowders. – X-ray-activated near-infrared luminescent nanoparticles are considered as new, autofluorescence-free alternative optical probes, while both their excitation and emission possess a high penetration efficacy in vivo. We reported silicon carbide quantum dot sensitization of trivalent

chromium-doped zinc gallate nanoparticles with enhanced near-infrared emission upon X-ray and UV–vis light excitation [6]. We have found that a $ZnGa_2O_4$ shell is formed around the SiC nanoparticles during seeded hydrothermal growth, and SiC increases the emission efficiency up to 1 order of magnitude due to band alignment that channels the excited electrons to the chromium ion.

2020

Technical development of the crystal growth laboratory. — For the sake of standardization, four computer-controlled Czochralski crystal growth apparatuses have been updated using identical parts and upgraded software. New high-precision temperature controllers and improved digital balances are now well integrated with the high speed computers.

Lithium niobate nanocrystals. – Tm^{3+} and Yb^{3+} double-doped $LiNbO_3$ nanoparticles with various rare earth concentrations were prepared by the ball-milling method. Three processes were compared: wet, dry and surfactant-assisted dry milling. For wet milling, water was used as dispersant causing significant alkalinity of the particles. The obtained average particle size was 10 nm. Using dry milling, the production of alkalinity could be avoided and a size of 40 nm could be reached (Figure 1.). The first experiments using surfactant-assisted dry milling produced a homogeneous size distribution in the sample with average particle diameter of 100 nm. The particles were characterized by Dynamic Light Scattering and Scanning Electron Microscopy methods.

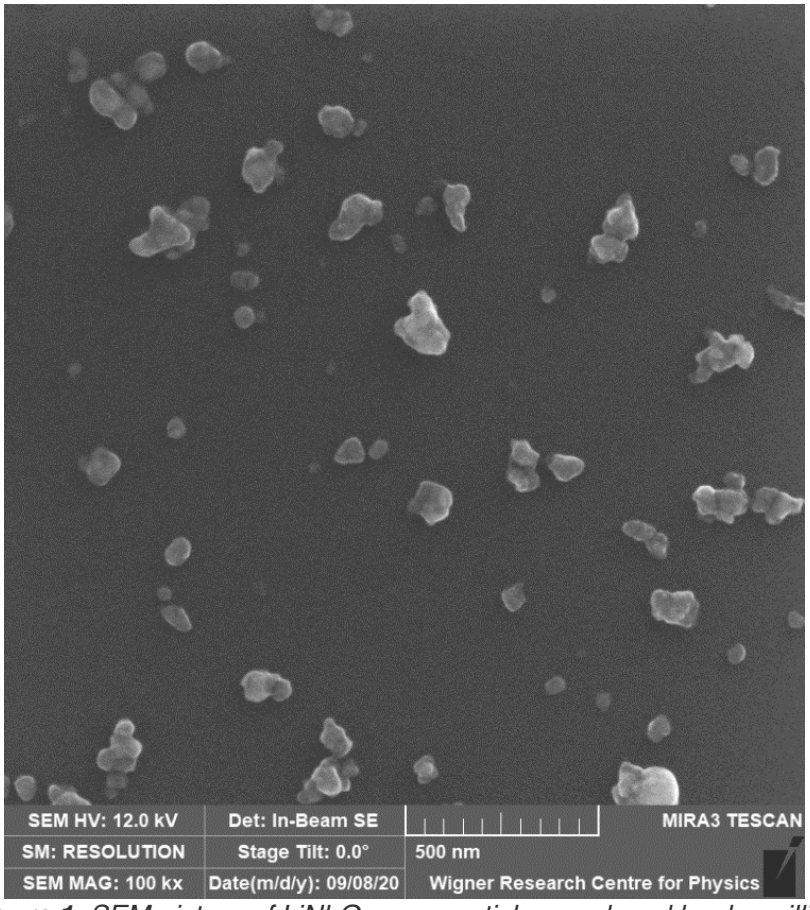

Figure 1. *SEM picture of $LiNbO_3$ nanoparticles produced by dry milling*

Pulse-reflectometry on $LiNbO_3$ nanocrystals. — Time-resolved nonlinear optical sum-frequency generation (SFG) of two differently colored, infrared laser pulses has been studied by nonlinear diffuse fs-pulse reflectometry using $LiNbO_3$ nanoparticle-pellets. The visible SFG emission exhibits an asymmetric pulse shape in the time domain which is explained within the framework of light propagation in random media. The analysis of the spectro-temporal data set indicates that $LiNbO_3$ nanoparticle-pellets can be used for an alternative type of an optical correlator, e.g. for the determination of a pulse's chirp parameter [1].

Terahertz time-domain spectroscopy of Mg-doped stoichiometric $LiNbO_3$. —Terahertz time-domain spectroscopy measurements were performed on Mg-doped stoichiometric $LiNbO_3$ crystal using ordinary and extraordinary polarization in the 4-460 K temperature range. The absorption coefficient and refractive index spectra were recorded in the frequency range from 0.5 to 1.8 THz. The importance of temperature effects for the design and adjustment of terahertz sources has been pointed out given the goal to maximize the optical-to-THz conversion efficiency [2].

SEM investigation of the defect structure of Mg doped $LiNbO_3$ single crystals. — This is an ongoing program to establish the relationship between crystal composition and defect structure for finding the optimal composition in the Li_2O-Nb_2O_5-MgO ternary system, suitable for the growth of high quality crystals. SEM investigations reveal defect structures containing grain boundaries on the z-cut surface. Line profile analysis at the edge of the structure shows an abrupt change of the O/Nb ratio and the appearance of impurities.

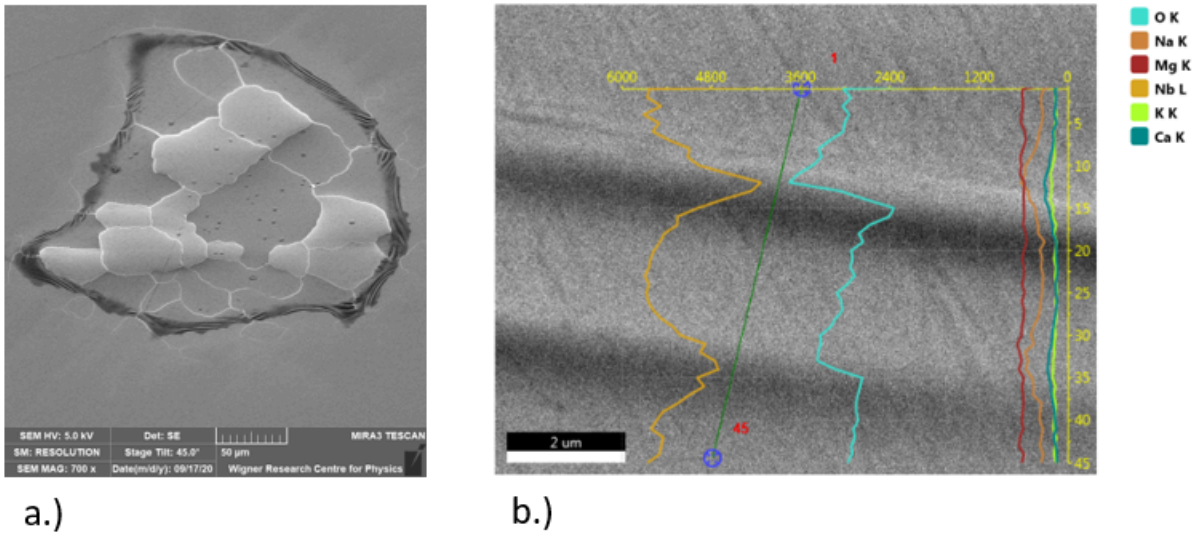

Figure 2. *SEM image of the defect structure of a $LiNbO_3$:Mg crystal containing grain boundaries (a), and line profile analysis showing the alteration of the O/Nb ratio and the presence of impurities at the edge of the structure (b).*

Laser-pulse induced luminescence in $LiNbO_3$. — Photoluminescence (PL) processes in Mg-doped $LiNbO_3$ have been interpreted based on a general model of coupled decay channels of radiative and non-radiative types having differently time-dependent decay kinetics. The considered model explains all features of the experimentally observed polaronic and excitonic scenarios, including lifetimes, stretching, and quenching behavior. Assuming exciton pinning on various dipolar defects predicted by defect incorporation theories clarifies the complex branching structure of the decay process, comprising at least two radiative and several non-radiative channels, and explains also domain contrast effects in PL [3].

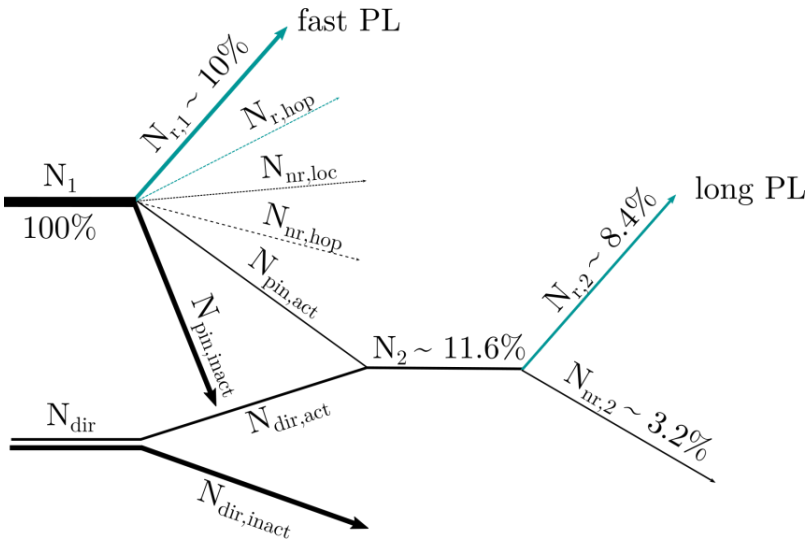

Figure 3. *Channel chart of decaying excitons in Mg doped $LiNbO_3$, hopping to or directly generated at dipolar defects.*

Spectral hole burning in $LiNbO_3$:Yb and LYB:Yb. — Spectral hole burning experiments have been carried out on Yb doped $LiNbO_3$ and $Li_6Y(BO_3)_3$ by using an actively frequency stabilized external cavity diode laser to

confirm previous results on homogeneous linewidth, where an unknown laser linewidth could have limited the resolution. The spectral hole width of 2 MHz obtained at 4.2 K did not differ significantly from those extrapolated from previous measurements at 8 K and above.

Rare earth ions in lithium yttrium orthoborate ($Li_6Y(BO_3)_3$, LYB) single crystals. — Beside the cooperative luminescence (CL) signal of Yb^{3+} ion pairs successfully generated in LYB:Yb crystal, emission bands of Eu^{3+}, Dy^{3+} and Tm^{3+} impurities were also identified in the wavenumber range of 12000-27000 cm^{-1} using laser excitation at 364 nm wavelength in a LYB:Yb (20 mol%) sample at room temperature. The presence of the excess rare earth ions helps the investigation of different APTE processes (acronym derived from French Addition de Photons par Transferts d'Energie) due to excited Yb^{3+} ions.

Designing and building a confocal microscope. — The project of building a confocal microscope has arrived to its final stage. An actively stabilized tunable external cavity diode laser setup with a variable frequency double-pass acousto-optical modulator unit has been built on the vibration isolated optical table connected to the microscope. The stabilization is based on a 50 mm long plano-concave Fabry-Perot interferometer, a Sacher LB2005 modulator/demodulator and a Sacher LB2001 servo controller unit. A light isolating box has also been designed to shield the setup.

Analytical methods for environmental and advanced materials. — Seasonality of atmospheric gases, water-soluble, elemental and black carbon content of size-segregated particulate matter (PM) was studied over the Belgian North Sea and a coastal site [4]. Aerosols from ship exhaust contributed mostly to fine PM and less to medium-sized PM, whereas sea spray and mineral/soil components were dominating in coarser fractions. More ship emission related components occurred in fine and medium PM in winter, when gaseous pollutants were peaking as well, thus supporting the more intense formation of secondary aerosol. As a general tendency: the higher the aerosol mass on the open sea with ship traffic, the higher the PM mass at the coast. The composition of total air PM was monitored at sites with industrial, commercial, heavy trafficked and mixed urban influence in Dar es Salaam [5]. Elemental ratios were useful for diagnostic purposes, i.e., PM source identification. Significant increases in air levels of As, Br, Cr, Cu, Mn, Ni, Pb and Zn were observed, when compared to data before 2010. Air quality indices and AIRQ+ modeling predict increases of negative health effects for sensitive groups of the local population.

References:

[1] doi.org/10.1002/adpr.202000019
[2] doi.org/10.1364/OME.384997
[3] doi.org/10.1088/1361-648X/ab9c5b
[4] doi.org/10.1016/j.aeaoa.2020.100077
[5] doi.org/10.1007/s11869-020-00832-8
[6] doi.org/10.3390/cryst10090780

2019

LiNbO3 nanocrystals. — The particle and grain size of lithium niobate nanocrystals prepared by ball-milling have been characterized by dynamic light scattering and powder X-ray diffraction methods . Milling resulted in sample darkening due to mechanochemical reduction of Nb(V) via polaron and bipolaron formation, oxygen release and Li2O segregation, while subsequent oxidizing heat-treatments recovered the white color with the evaporation of Li2O and crystallization of a LiNb3O8 phase instead. Raman spectroscopy, X-ray diffraction, optical reflection measurements and coulometric titration have been used to follow the phase transformations occurring during both the grinding and the post-grinding heat treatments.

Hydroxyl ions in $LiNbO_3$ single crystals. — Vibrational bands of hydroxyl ions (OH-) have been observed in stoichiometric $LiNbO_3$ (sLN) single crystals for transition metal ion (Fe^{3+}, Cr^{3+}, Ti^{4+}) dopants above a threshold concentration, and attributed to the stretching vibration of OH^- ions in M_{Nb}^{n+}– OH type complexes, where the dopant *M* occupies a Nb site . The observed vibrational frequencies of the OH^- ions and their polarization dependences agree well with the model established earlier for LiNbO3 doped with optical damage resistant and rare-earth ions, confirming its general validity (see Fig. 1). Hydroxyl ions are the most convenient probes for the detection of the change of any dopant incorporation from Li to Nb site at the threshold concentration

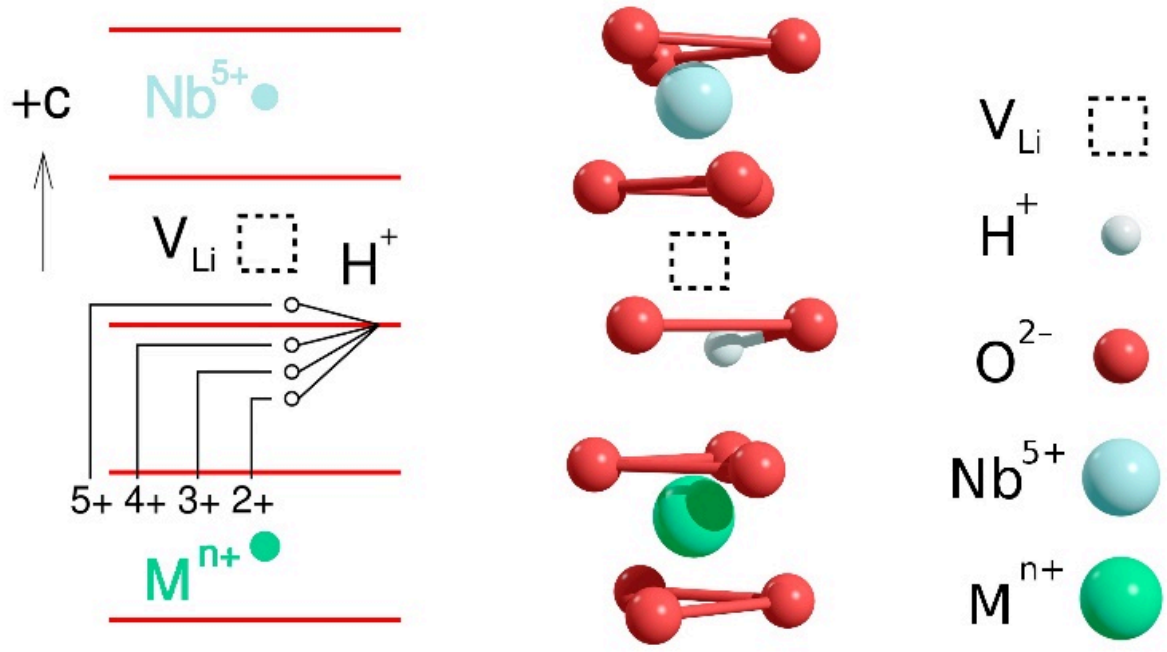

Figure 1. *Schematic drawing of the* OH- *location in* Mn+- *doped sLN crystals.*

Laser-pulse induced optical transients in LiNbO3. — While fast transient near IR absorption in LiNbO3 is due to polaron decay, photoluminescence processes in Mg-doped LiNbO3 observed in three different time domains could be identified to correspond to various excitonic species, i) mobile or frozen-in self-trapped excitons emitting on the microsecond scale, ii) excitons trapped on charge-compensated complexes of NbLi antisites and decaying on the nanosecond scale, and iii) excitons pinned on charge-compensated dipolar complexes formed by Mg dopants yielding transients on the second scale . Similar or even longer transients of the absorption in the blue range in Mg or Fe doped LiNbO3 have also been assigned to pinned excitons, attributing the exorbitant lifetimes to the defect-pinned outstretched excitonic structure. Pinned excitons have been shown to form via hopping of self-trapped excitons or by their direct generation at dipolar defects. Absorption bands observed earlier in the UV-edge region can accordingly be assigned to direct pinned-exciton generation on dipolar defects. Polaronic and excitonic hopping-pinning scenarios together allow for a coherent explanation of all optical transients with relevance for a large class of complex systems.

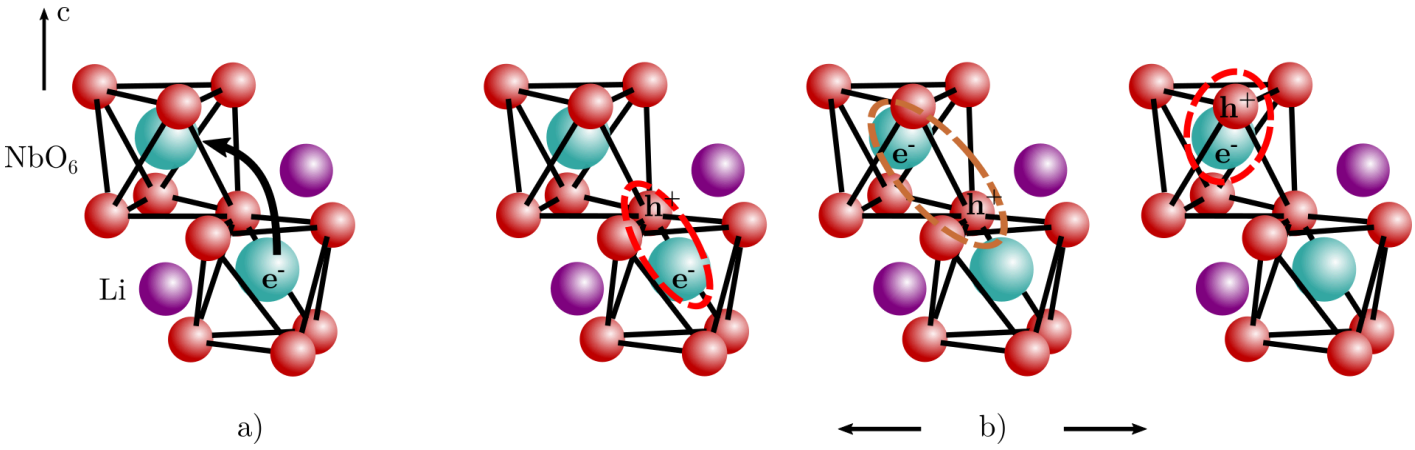

Figure 2. *Hopping of polarons (a) and self-trapped excitons (b) in LiNbO3. Both processes are essentially defined by the hopping of the electron between Nb sites since the additional hole constituent of the exciton moving in a close-packed oxygen sublattice has a larger mobility.*

Spectroscopy of lithium yttrium orthoborate (Li6Y(BO3)3, LYB) single crystals. — Emission bands of Dy3+ impurity excited by an energy transfer upconversion (ETU) process via neighboring Yb3+ ions were revealed in the luminescence spectra of LYB:Yb(20mo%) using continuous infrared laser excitation. A theoretical model based on the saturation absorption effect was developed and successfully applied (Fig. 3) to describe the intensity and temperature dependencies of the cooperative luminescence (CL) of Yb3+ pairs in the same crystal. The temperature dependence of the obtained saturation intensity parameter shows good agreement with previous independent calculations in the literature.

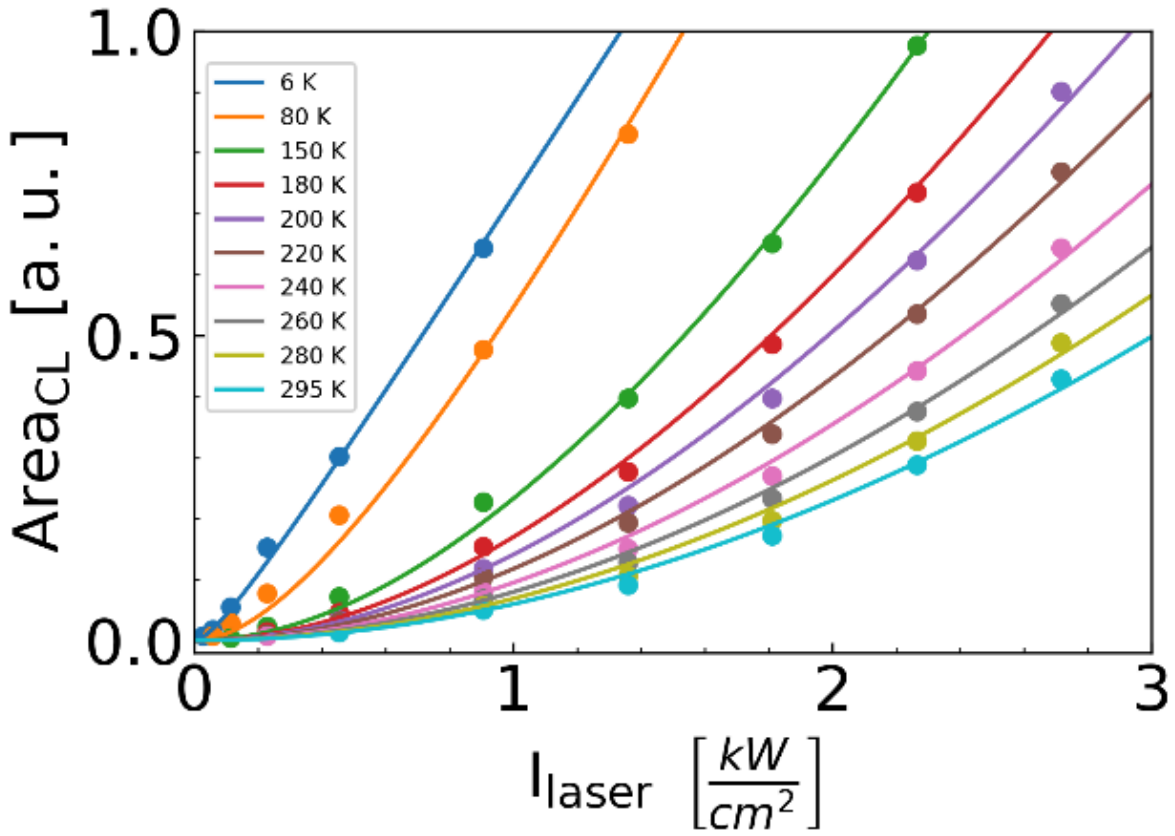

Figure 3. *Simultaneous fitting to the power dependence of integrated CL intensity of the Yb3+-pairs measured at different temperatures in a 20 mol% Yb-doped LYB crystal using continuous wave laser excitation at a wavelength of 972 nm.*

Time-resolved luminescence spectroscopy of Tm-Yb co-doped LYB single crystals and nanocrystals. — The energy levels of Tm3+ ions in Li6Y(BO3)3 grown by the Czochralski method have been determined by absorption and luminescence spectroscopy. In Tm and Yb co-doped crystals an energy transfer process from the excited Yb3+ to the Tm3+ ions has been observed. Both Tm and Yb co-doped LYB single crystals and NaYF4 nanocrystals have been investigated with a time-resolved luminescence spectroscopy setup consisting of a tunable external-cavity IR diode laser, an acousto-optical modulator, a low-pass filter, a monochromator and a single-photon counter. For both samples, a second order intensity dependence of the saturation luminescence intensity has been found at 800 nm, indicating a two-photon excitation process. Further investigations for the interpretation of the qualitatively different pump intensity dependences of the time parameters found for these two materials, and the assessment of similar crystals as possible single-photon sources are in progress.

Designing and building a confocal microscope. — After the construction of the mechanical backbone of a new confocal microscope last year, this year optical components were assembled for laser excitation and the detection of photons emitted from a single-photon source. As a significant step forward the computer control of the microscope has been achieved by using the LabVIEW software.

Analytical methods for environmental, biological and advanced materials. — Electric IR-heating systems operated in wooden and stone churches have been shown to produce an uneven air pollutant and water vapor distribution indoors due to ventilation induced by warm air, which can have a detrimental effect on the displayed works of art . New atomic spectrometric methods for Cd quantitation in cells of various living forms were developed and applied to study the transporter function of the ABCB6 protein playing an important role in Cd detoxification . An electrolyte cathode atmospheric glow discharge operated in water vapor atmosphere has been built and studied for on-line, optical emission monitoring of elements present in natural water sediments. Spectral interferences were suppressed and signal-to-noise ratios for several elements have been improved.

2018

LiNbO3 single and nanocrystals. – A cost-effective, crucible-rest-refilling technology has been developed for the serial high-temperature top-seeded solid solution growth of high-quality Mg-doped stoichiometric LiNbO3 crystals, resistant to optical damage. Nanocrystals have been prepared by shaker and planetary milling from LiNbO3 crystals of congruent composition. While dry shaker milling resulted in particle sizes of a few hundred nm

with gray coloration due to partial reduction, wet planetary milling with 0.1 mm zirconia balls in zirconia vial produced the desired 10-20 nm size.

Using EXAFS spectroscopy, the incorporation of Er, In and Hf dopants was determined in LiNbO3 single crystals. Er mostly substitutes at the Li site with a small fraction at Nb site, with little change between stoichiometric and congruent LiNbO3. In ions also primarily substitute at the Li site in congruent LiNbO3; Hf appears to be nearly evenly distributed between Li and Nb sites. While charge-compensating defects are required, self-compensating schemes are not consistent with the data.

Using transient absorption spectroscopy in the mid/near infrared region in Mg-doped LiNbO3 crystals, the dissociation and thermalization of hot excitons produced by 100 fs laser pulses at ~2.5 eV with power up to 2 PW/m2 was shown to occur on a ~200 fs timescale leading to localized Nb4+ small polarons via an interim state attributed to electrons without local lattice relaxation. Exciton hopping and pinning on dipolar crystal defects have been demonstrated to play decisive roles in the luminescence components observed under pulsed excitation.

Spectroscopy of lithium yttrium orthoborate (Li6Y(BO3)3, LYB) single crystals. – Undoped LYB single crystals grown by the Czochralski method were investigated for their suitability for optical applications. Two bands near the UV absorption edge, at about 220 and 240 nm, have been found with no and a small difference in their amplitudes between the top and bottom parts of the crystals for stoichiometric and off-stoichiometric compositions, respectively. XRF and luminescence measurements revealed no contamination of the crystals, so the UV bands can be attributed to intrinsic defects distributed more homogeneously in stoichiometric crystals.

The amplitude of the lowest energy absorption band of Yb3+ ions in LYB single crystals was observed to increase upon cooling from 300 to 9 K by more than two orders of magnitude, while the halfwidth decreased to 0.16 cm-1. This strong temperature dependence explains the anomalous behavior of the time and intensity dependence of the cooperative pair emission previously investigated in similar crystals. Cooperative pair absorption was successfully demonstrated in a Li6Yb(BO3)3 crystal (where Yb is a matrix ion) in the same wavenumber range where pair emission in LYB:Yb was observed. Spectral hole burning in LYB doped with monoisotopic 166Er3+ ions has been investigated in magnetic fields. For coaxial field orientation, two pairs of spectral side holes were detected with a magnetic sensitivity of about ±75 and ±177 MHz/mT, while these holes split to more components in the case of a general direction of the magnetic field.

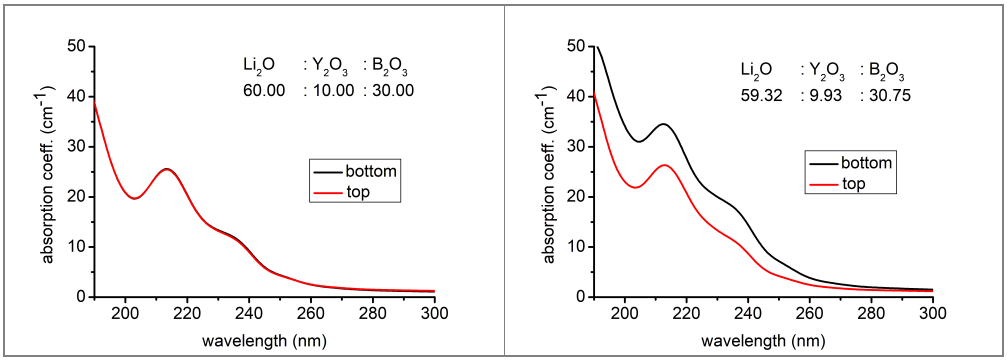

Figure 1. *UV spectra of slices cut from the top and bottom parts of stoichiometric and off-stoichiometric LYB crystals, the latter showing changed amplitudes.*

Designing and building a confocal microscope. – A new confocal microscope has been designed from the ground up to detect photons from a single-photon source. The samples mounted in a cryostat can be moved by synchronized motors. Optimal optical components were chosen for laser excitation and the detection of the emitted photons. A setup comprising a monochromator and a photon counter has also been developed for testing and optimizing solid state samples and suspensions.

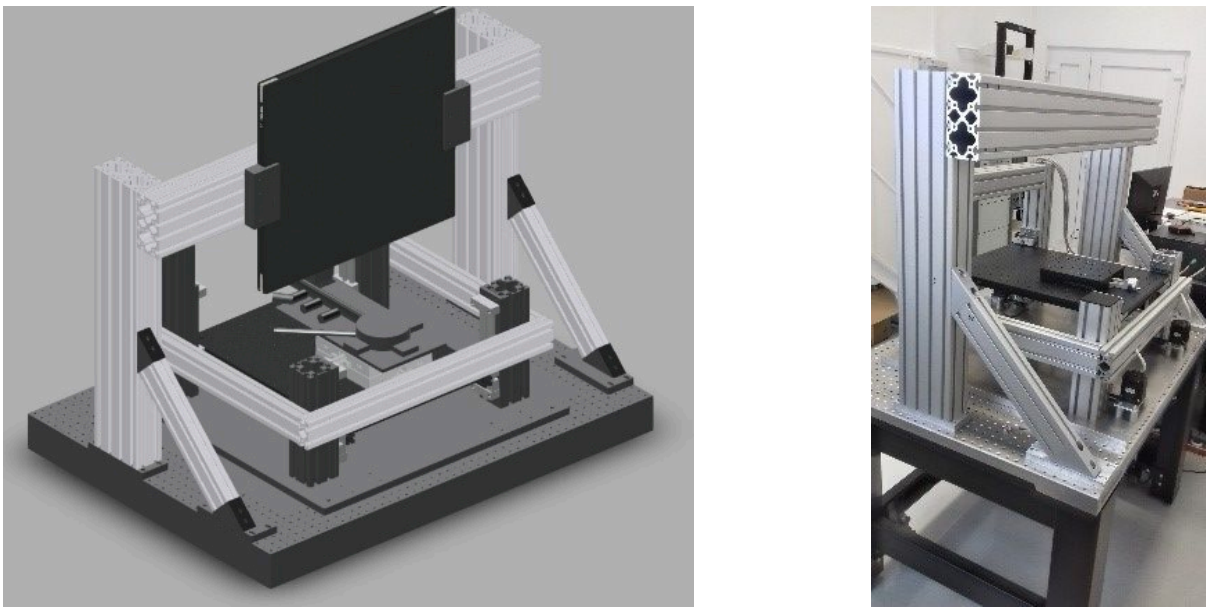

Figure 2. *Design (a) and realization (b) of the confocal microscope stand.*

Analytical methods for environmental and advanced materials. – An open-air ELCAD-OES system fitted with a low-resolution mini UV spectrometer has been built for on-line monitoring of river sediments. By correcting for structured molecular background emissions, the signal-to-noise ratios for Cd, Cu, Mg, Mn, Ni, Zn, etc. can be significantly improved. Acidic pressure digestion and flame atomic absorption methods were developed for major and minor constituents (Al, Ca, Fe, K, Mg, Mn, Na, Si, Sr, Ti) of alginite, which is an environmentally and agriculturally strategic mineral in Hungary.

2017

Crystal growth of niobates. — A series of Fe+Ti double-doped stoichiometric LiNbO3 (LN) crystals has been grown to optimize/balance photorefractive and wave-guiding properties. Rare-earth (Er, Nd, Yb) and transition-metal (Fe, Ti) doped over-threshold stoichiometric LN crystals have been grown for IR spectroscopic studies showing that these dopants (M) may also incorporate at Nb sites forming MNb - OH- -type complexes like optical-damage-resistant (Mg, Zn, In, Sc, Hf, Zr, Sn) ions.

Spectroscopy of lithium yttrium orthoborate (Li6Y(BO3)3, LYB) single crystals. — Czochralski grown LYB:Dy crystals suitable for scintillator and laser communication systems (Fig. 1) have been characterized by temperature and polarization dependent FTIR absorption and luminescence measurements. Up to the 4I15/2 multiplet, all Stark levels split by low-symmetry crystal field could be determined. The most intense luminescence was detected at 577 nm (4F9/2 → 6H13/2 transition).

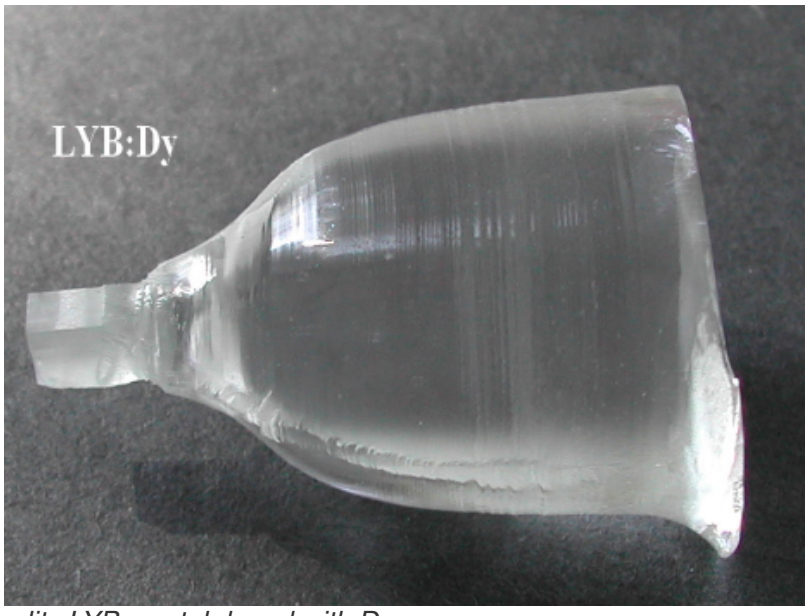

Figure 1. *High optical quality LYB crystal doped with Dy.*

Coherent Yb-pair emission in Li6Y1-xYbx(BO3)3 crystals (x=0.01, 0.05, 0.20) was successfully generated using laser excitation at »972 nm. At 6 K, the emission showed a detailed structure containing at least 13 band components in the 470-540 nm range. The laser intensity dependence of the integrated area of the spectra was explained by an energy transfer mechanism via Yb3+ chains in the crystal lattice.

Spectroscopy of the tissue-equivalent dosimeter material lithium tetraborate (LTB). —Luminescence studies of Mn doped LTB single crystals complemented by EPR analysis in the 33 GHz Q-band revealed rechargeable Mn2+ centres incorporated in the lithium sublattice, compensated by mobile lithium vacancies. Both electrons and holes created by ionising radiation are trapped by Mn2+ centres, their recombination accounting for the thermoluminescent readout of the radiation dose.

Spectroscopy of LiNbO3:Yb nano-powders. — LN nano-powders have been prepared by high-energy ball milling from bulk crystals, using alumina, steel or tungsten carbide vials. The type of mills, number of balls (1 or 2), milling time and the ball-to-powder ratio has been varied to produce the smallest grain size. After resonant irradiation at λ=980 nm, a fluorescent signal with a lifetime of 0.5 ms at »40 K, but surviving also at RT was found in a LiNbO3:Yb nano-powder with a characteristic grain size of 390 nm. Using a saturation spectroscopic method in KBr-LiNbO3:Yb pellets with characteristic size of 390 nm, the population relaxation kinetics and magnetic field splitting of the spectral hole was determined for the 2F7/2 – 2F5/2 transition of Yb3+. The same processes were studied for 70 nm pellets as well, but only a single strong spectral hole component with a lifetime longer than 10 h was found instead, that could only be erased by a 30 min annealing of the sample above 90 K.

Transient absorption of small polarons and excitons in LiNbO3:Mg. — Picosecond absorption in the 0.3-1.05 eV *mid-infrared* region induced by 100 fs pumping pulses with 2.5 eV photon energy was attributed to free electrons originating from hot electron-hole pairs undergoing phonon-assisted dissociation and cooling, as well as their subsequent trapping as Nb4+ polarons at regular Nb sites. The concentrations of hot, cold, and polaronic charge carriers could be derived based on a kinetic model. Long-lived absorption in the *near infrared and visible* region could be interpreted as due to the survival of trapped polarons and pinned excitons near lattice defects, respectively (Fig. 2).

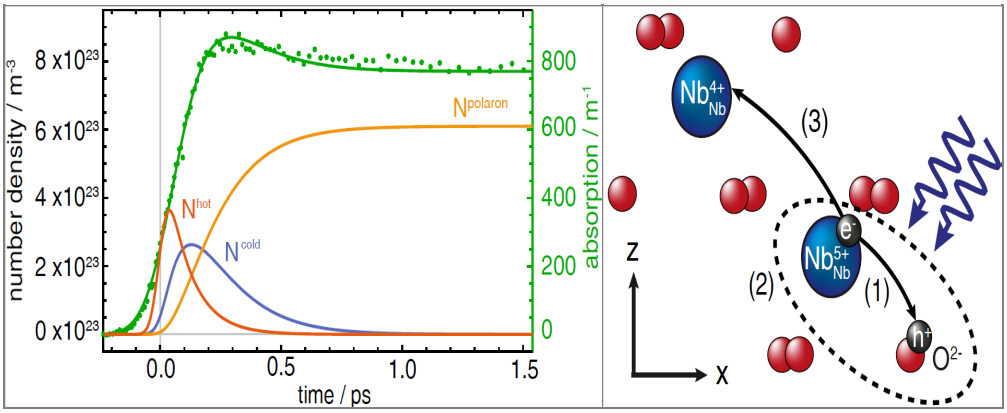

Figure 2. *Left: subpicosecond pulse-induced two-photon absorption in LiNbO3:Mg (green) and the resulting number densities of hot, cold and polaronic carriers (orange, blue and yellow lines, respectively). Right: early recombination (1), excitonic stabilisation (2) and dissociation (3) of hot electron-hole pairs located on neighboring matrix ions of the LiNbO3 lattice.*

Dielectric parameters of lithium tantalate (LiTaO3) in the terahertz range. — The refractive indices and absorption coefficients of congruent, stoichiometric and 0.5 or 1.0 mol% Mg-doped LiTaO3 crystals have been investigated using polarization dependent terahertz time-domain spectroscopy in the 0.3-2.0 THz range. The data were successfully fitted by a three-term Lorentz oscillator model. Stoichiometry was shown to have a significant influence, while Mg had a much smaller effect. LiTaO3 can be a promising THz generator material due to the lack of the three-photon absorption at 800 nm.

Analytical methods for environmental and advanced materials. — The distributions of mass, water-soluble inorganic salts and mineral elements of size-segregated aerosols, precursor gaseous pollutants, black carbon, and nanoparticles over the Southern North Sea have been studied. The nano-aerosol count, originating from ocean-going ships, peaked at lower diameters (»28 nm) than those observed for smaller (e.g. fishing) boats (45-50 nm) and depended also on weather conditions.

Solid phase extraction with high-resolution continuum-source graphite-furnace atomic absorption spectrometry has been developed for speciation of inorganic As in geothermal, well and pretreated water samples from four Hungarian waterworks. Total As in well waters varied between 40-120 µg/L. Occurrence of As(III) in well waters exceeded 80% of the total As, while As(V) was predominant (≈90%) in pretreated waters, but below the health limit value of the 98/83/EC Council Directive (10 µg/L).